Magnetic nanoparticle-molecular imprinted polymer: a new impedimetric sensor for tributyltin detection.

Alejandro Zamora Gálvez,[a,b‡] Carmen C. Mayorga-Matinez,[a‡] Claudio Parolo,[a] Josefina Pons,[b] Arben Merkoçi[a,c]*

[a] *Nanobioelectronics & Biosensors Group, Catalan Institute of Nanoscience and Nanotechnology (ICN2), CSIC and The Barcelona Institute of Science and Technology, Campus UAB, Bellaterra, Barcelona, 08193, Spain.*

[b] *Departament de Química, Universitat Autònoma de Barcelona, 08193, Bellaterra (Barcelona), Spain.*

[c] *ICREA, Pg. Lluís Companys 23, 08010 Barcelona, Spain.*

* *E-mail: arben.merkoci@icn2.cat*

[‡] *These authors contributed equally.*

Abstract

Recently, molecular imprinted polymers (MIPs) were extensively used for separation and identification of specific molecules, replacing expensive and unstable biological receptors. Nonetheless, their application in electrochemical sensors has not been sufficiently explored. Here we report the use of a MIP as a specific receptor in a new highly sensitive tributyltin (TBT) electrochemical sensor. The sensor combines the specificity, pre-concentration capability and robustness of molecular imprinted polymer attached onto magnetic nanoparticles with the quantitative outputs of impedimetric measurements. The proposed device detects TBT in a concentration range of 5 pM to 5 μM with a low limit of detection (5.37 pM), which is lower than the one recommended for TBT in sea water by the US Environmental Protection Agency (EPA). We believe that this new electrochemical sensor can play an important role in the monitoring of the quality of sea and fresh waters worldwide.

Keywords: Electrochemical impedance spectroscopy, pollutants, electrochemical sensor.

1. Introduction

For decades, the pesticide tributyltin (TBT) has been an important additive in antifoulant paints to prevent the growth of marine organisms on the hulls of large ships. Eventually, this highly toxic pesticide leaks in the aquatic environment causing immuno-suppression and imposex in snails and bivalves, inhibiting the growth of several marine organisms, and inducing immunotoxic, hepatotoxic, and neurotoxic effects in fish and mammals, with potential effects even for humans [1–3].

Nowadays, the typical methods to detect pesticides, including TBT, are chromatography separation [4–6], gas chromatography [7–9], electron-capture detector [10], flame ionization detector and mass spectrometry [11]. These techniques reach low limits of detections (LOD) and have high reproducibility, but require extensive purification, expensive equipment and trained users [12]. During the past few years, electrochemical sensors showed to be a user-friendly and miniaturized alternative for pesticides detection.[13] Nevertheless, they normally use bio-receptors (aptamers, antibodies, enzymes) [13–15], which can be instable, non-specific, and expensive. Recently, we and others used molecular imprinting polymers (MIPs) for the development of specific methods for the detection of different kinds of molecules such as fenitrothiol, organochlorine, and heptachlor [14–16].

In this paper we present a new sensing platform for the detection of TBT based on MIP technology. Our system is based on the use of screen printing electrodes in conjunction with MIP-Fe_3O_4 nanoparticles (NPs) composite [15–17] as a specific receptor for TBT. Thanks to the use of electrochemical impedance spectroscopy, we managed to quantitatively detect TBT in fresh and sea water (see scheme in Figure 1A) [14,16–18].

2. Experimental

Chemicals and Materials

Tributyltin hydride, (3-Aminopropyl) trimethoxysilane, acryloyl chloride (C_3H_3ClO), $FeCl_2$•$4H_2O$, $FeCl_3$•$6H_2O$, ammonium hydroxide (NH_4OH), toluene anhydrous, potassium carbonate (KCO_3), ethanol, acetonitrile, ethylene glycol dimethacrylate 98%, 2,5-Bis(tert-butylperoxy)-2,5-dimethylhexane 90%,

sodium hydroxide and methanol were purchased from Sigma Aldrich. Transmission electron microscope (TEM) FEI TECNAI G2 F20 (USA), X-ray photoelectron spectrometer Phoibos 150 analyzer (SPECS GmbH, Berlin, Germany) in ultra-high vacuum conditions (base pressure 1x 10^{-10} mbar). The infrared spectroscopy was performed by IR-ATR model IR Tensor 27 (Bruker). Homemade SPE, which fabrication method was reported previously [14].

Synthesis of molecular imprinted MIP-Fe_3O_4NPs composite

For the synthesis of the MIP-Fe_3O_4NPs composite we modified a protocol previously reported by Zhu et al. [19]. A mixture of $FeCl_2$•$4H_2O$ 0.02 g/mL and $FeCl_3$•$6H_2O$ 0.054 g/mL was prepared and stirred under nitrogen to prevent the formation of Fe_2O_3. After that, 20 mL of ammonium hydroxide 25 M was added and the reaction was refluxed at 80 °C for 40 min. The solution was decanted and washed three times with MilliQ water to remove any unreacted reagent. The Fe_3O_4NPs were dried in a vacuum at 45 °C. All the next steps were performed under Schlenk line, to increase the stability of the compounds. Then, 0.1 g of Fe_3O_4 NPs was dissolved in 150 mL ethanol/water 14:1 and 50 µL 4.27 mM of amino propyl triethoxysilane (APTS) was added drop by drop, under continuous stirring during 7 h at room temperature and nitrogen ambient. Following by washing steps with absolute ethanol (5 times), and dried in vacuum. 0.1 mg of APTS- Fe_3O_4NPs and 0.5 g of K_2CO_3 were dispersed in 50 mL of toluene under ultrasonic ice bath during 30 min and 1 mL 0.012 M of acryloyl chloride was added and the flask was sealed, the mixture was under vigorous stirring for 12 h at room temperature. Next, the product was collected by application of an external magnetic field and rinsed three times with toluene, ethanol and acetonitrile, then the product was dried in vacuum conditions.

The modified Fe_3O_4 NPs (0.1 g) and 269 µL of tributyltin hydride (TBTH) were dissolved in 40 mL 19 M of acetonitrile and stirred for 6 h until the template-monomer was formed. Then 4.14 mL at 5.3 M of ethylene glycol dimethacrylate (EGDMA) and 9.35 µL 3M of 2,5-bis(tertbutyl peroxy)–2,5 dimethyl hexane were added in the solution. The solution was placed in the ultrasonic ice-bath for 5 min then was heated at 50 °C for 5 h and polymerized at 65 °C for 20 h. Finally the mixture was heated at 85°C for 5 h to assure complete polymerization. The reaction was purged with nitrogen and stirred. The resultant product

was rinsed five times with a mixture of methanol-dichloromethane (4:1) and finally the resulted product was extracted using Soxhlet for 60 hours in presence of 0.3 M NaOH dissolved in methanol, the final product was dried under vacuum conditions. Although the synthesis of the MIP-Fe_3O_4NPs composite requires long time, the final amount that is obtained (ca. 5 grams) is enough to perform over 100 measurements.

Electrochemical measurements

For TBT detection, we incubated solutions of different TBT concentrations with 10 mg/mL of MIP-Fe_3O_4NPs composite under stirring conditions for 2 h at room temperature. Afterward, 10 µL of the above suspension was drop casted onto the working electrode area of the SPE and TBT/MIP-Fe_3O_4NPs composite was accumulated onto the working electrode area with the help of a permanent magnet placed underneath. Then electrochemical impedance spectroscopy (EIS) was performed in 1 mM $[Fe(CN)_6]^{3/4}$ with 0.1 M KCl adding 50 µL of this solution over the working electrode. A sinusoidal potential modulation of ±20 mV amplitude in the 0.1 Hz to 100 kHz frequency range was superimposed onto the formal potential (0.24 V vs. Ag/AgCl) of the redox couple, $[Fe(CN)_6]^{3/4}$. For sea water measurements, we filtered the samples using a 0.05 µm VMWP filter to extract bigger compounds and impurities.

3. Results and discussion

Before applying MIP-Fe_3O_4NPs composite for TBT detection, we characterized it using TEM, IR, XPS. We used TEM to study the synthetized Fe_3O_4NPs, which had a diameter of 20.05 ± 4.37 nm and a good homogeneity (as shown in Fig. 1B), in line with previously reported synthesis [20,21]. Upon modification with the MIP, we observed some Fe_3O_4NPs aggregation (probably due to the polymerization process) [22], which increased the apparent diameter of the Fe_3O_4NPs to 59.77±7.15 nm (Fig. 1C). The aggregation of Fe_3O_4 NPs should not negatively affect the sensor behavior, since their only role is to accumulate the MIP on the working electrode surface (upon inducing a magnetic field with a permanent magnet), for this reason we refer to MIP-Fe_3O_4NPs composite, rather than just MIP-Fe_3O_4NPs. In order to confirm the incorporation of the Fe_3O_4NPs into the MIP, we magnetically separated the samples from their solutions

before characterizing them with IR spectroscopy. Figure 2A shows how the characteristic peaks of the MIP in the IR spectra (i.e. C-H, C=O, Si-O, C=C-H δ and Si-CH) appeared just in the MIP- Fe_3O_4NPs composite spectrum and not in the one of bare Fe_3O_4NPs, suggesting that the Fe_3O_4NPs were included into the polymer structure. We also characterized the composite and the bare nanoparticles with X-ray spectroscopy. The survey spectrum (Fig. 2B) of MIP- Fe_3O_4NPs composite shows the enhanced signals from O 1s, C 1s and Si 2p peaks in comparison of survey spectrum of Fe_3O_4NPs, confirming the formation of MIP- Fe_3O_4NPs composite. Fig. 2C shown the high resolution signals for the regions of O 1s, C 1s, Si 2p, Fe 2p and Ni 1s of MIP- Fe_3O_4NPs composite. Moreover, the specific surface was investigated by BET analysis and the obtained surface area for the MIP- Fe3O4NPs (59.77±7.15 nm) is 65 m^2/g (see Fig. 2D).

Once proved the formation of the MIP- Fe_3O_4NPs composite, we verified that the MIP could actually bind the TBT using EIS. Figure 3A shows the Nyquist spectra of bare (SPE), MIP- Fe_3O_4NPs and MIP-Fe_3O_4NPs incubated with 5 µM TBT. The resulted R_{ct} for the MIP- Fe_3O_4NPs composite is 0.65 kΩ, which indicates a low resistivity compared with the R_{ct} of the bare electrode of 15-20 kΩ. We think that there are two main components inducing this low R_{ct}: the catalytic activity of Fe_3O_4NPs [23,24] and the enhanced electrode effective area due to the presence of Fe_3O_4NPs. After the incubation of MIP-Fe_3O_4NPs with 5 µM TBT, the recorded signal is 1.66 kΩ. This enhanced Rct confirms the binding between of MIP-Fe_3O_4NPs and TBT, because the negative charge from the tributyltin hydride [25] acts as an electrostatic barrier between SPE and the redox mediator. This was confirmed by Zeta-potential experiments (Fig. 3B). A gradual shift to negative values was observed when the MIP-Fe_3O_4NPs is connect with TBT.

To verify that the signal change upon addition of TBT was specific, we performed the same measurements using NIP- Fe_3O_4NPs composite (non-imprinted polymer). We challenged our sensor with four different solutions: MIP- Fe_3O_4NPs composite, NIP- Fe_3O_4NPs composite, MIP- Fe_3O_4NPs composite with 5 µM TBT, and NIP- Fe_3O_4NPs composite with 5 µM TBT (see Figure 3B). The R_{ct} obtained using NIP- Fe_3O_4NPs composite, both in the absence (0.63 ± 0.176 kΩ) and presence (0.82 ± 0.066 kΩ) of 5 µM TBT, were very similar to the one obtained using MIP- Fe_3O_4NPs composite in the absence of TBT (Fig. 3B) and the imprinted factor using the equation (1) is 5.315. These observations suggest that the change

observed is induced by the specific binding of TBT to the MIP and not by non-specific adsorption of the TBT onto the working electrode or the composite. The R_{ct} is obtained using Randles model modified with Warburg impedance (Zw).

$$IF = \frac{Rct_{MIP+TBT} - Rct_{MIP}}{Rct_{NIP+TBT} - Rct_{NIP}} \quad (1)$$

After proving that the sensors responded to the presence of TBT, we challenged it with different TBT concentrations. The calibration curve of the R_{ct} values as a function of TBT concentration is shown in Figure 3C, a linear range spanning 6 orders of magnitude, from 5 pM to 5 µM (r^2=0.97) with a limit of detection (LOD) of 5.37 pM and a limit of quantification (LOQ) of 17.9 pM are obtained. The LOD and the LOQ was calculated by 3 times or 10 times the s/m criteria respectively, where s is the standard deviation of the Rct of the lowest concentration of the TBT (3 repetitions) and m is the slope of the corresponding calibration graph. Both the LOD and LOQ of our sensor are smaller than the values recommended by the US Environmental Protection Agency: 1.45 nM (acute criterion) and 25 pM (chronic criterion) [26]. Moreover, the high concentration tested is 100 times upper than the maximum allowable concentration indicated by international agencies.

On the other hand, the sensor revealed high reproducibility with a relative standard deviation (RSD) of 17.8%, calculated as the mean of RSD obtained from five TBT concentrations and three replicates for each concentration. The selectivity of our sensor is tested using 5 µM monobutylin dichloride (MTB) and dibutylin dichloride (DTB). MTB and DTB represent a potential interference in the detection of TBT. The R_{ct} values for MBT and DBT are considerably lower than the one obtained using TBT, respectively: 0.44 ± 0.176 and 0.81 ± 0.066 kΩ. The TBT produced a signal 377% and 200% higher than the ones obtained using MBT and DTB, proving the high selectivity of our sensor for TBT (see Fig. 3 E).

Finally, we challenged the MIP-Fe_3O_4NPs composite with a recovery test. We compared two different concentrations of TBT (5 pM and 5 µM) in pre-filtered sea water samples (n = 3 for each sample) with the same concentrations of TBT in MilliQ water. The recovery percentages (eqn. 2) were 110.33% and

78.18%, respectively for 5 pM and 5 µM. The recovery percentages were particularly good considering the complexity of sea water matrix.

$$Recovery\ percentage = \frac{[TBT]_{Sea\ water}}{[TBT]_{MiliQ\ water}} x100 \qquad (2)$$

4. Conclusions

We presented the development of the first impedimetric sensor for detection of TBT based on MIP-Fe_3O_4NPs composite. This low cost and user-friendly sensor shows excellent analytical performance thanks to the synergy between magnetic nanoparticles and MIPs. Such coupling allowed an efficient separation and preconcentration of the analyte. On one side, it responded specifically to TBT, in comparison to similar compounds (MBT and DBT), on the other its LOD (5 pM) and LOQ (18 pM) were below the values recommended by the US Environmental Protection Agency: 1.45 nM (acute criterion) and 25 pM (chronic criterion). Compared to other TBT detection systems, it showed the widest range of response and one of the lowest LOD found in the literature[27,28]. The high sensitivity of this system is attributed to high selectivity of MIP implemented previously by Zhu et.al [19] and the high sensitivity of the EIS as reported before [29-33]. The results demonstrate that the MIP-Fe_3O_4NPs composite is a robust and stable receptor for the electrochemical detection of pesticides.

5. Acknowledgment

This work was supported by: The European Commission Program, FP7-OCEAN, SMS Project (613844) and MINECO (Spain, MAT2014-52485-P). ICN2 acknowledges support from the Severo Ochoa Program (MINECO, Grant SEV- 2013-0295). Nanobiosensors and Bioelectronics Group acknowledges the support from Secretaria d'Universitats i Recerca del Departament d'Economia i Coneixement de la Generalitat de Catalunya (2014 SGR 260).

6. References

[1] M.A. Farajzadeh, B. Feriduni, M.R.A. Mogaddam, Determination of triazole pesticide residues in edible oils using air-assisted liquid–liquid microextraction followed by gas chromatography with

flame ionization detection, J. Sep. Sci. 38 (2015) 1002–1009.

2] S. Murata, S. Takahashi, T. Agusa, N.J. Thomas, K. Kannan, S. Tanabe, Contamination status and accumulation profiles of organotins in sea otters (Enhydra lutris) found dead along the coasts of California, Washington, Alaska (USA), and Kamchatka (Russia), Mar. Pollut. Bull. 56 (2008) 641–649.

[3] B. Antizar-Ladislao, Environmental levels, toxicity and human exposure to tributyltin (TBT)-contaminated marine environment. A review, Environ. Int. 34 (2008) 292–308.

[4] M. Astruc, A. Astruc, R. Pinel, Specification of butyltin compounds by HPLC-ETAAS, Mikrochimica Acta, 109 (1992) 83–86.

[5] I.R. Pereiro, V.O. Schmitt, J. Szpunar, O.F. Donard, R. Lobiński, Speciation analysis for organotin compounds in biomaterials after integrated dissolution, extraction, and derivatization in a focused microwave field., Anal. Chem. 68 (1996) 4135–40.

[6] E. Turiel, A. Martin-Esteban, Molecularly imprinted polymers: towards highly selective stationary phases in liquid chromatography and capillary electrophoresis, Anal. Bioanal. Chem. 378 (2004) 1876–1886.

[7] X. Song, J. Li, S. Xu, R. Ying, J. Ma, C. Liao, D. Liu, J. Yu, L. Chen, Determination of 16 polycyclic aromatic hydrocarbons in seawater using molecularly imprinted solid-phase extraction coupled with gas chromatography-mass spectrometry, Talanta. 99 (2012) 75–82.

[8] J. Carpinteiro, I. Rodríguez, R. Cela, Applicability of solid-phase microextraction combined with gas chromatography atomic emission detection (GC-MIP AED) for the determination of butyltin compounds in sediment samples, Anal. Bioanal. Chem. 380 (2004) 853–857.

[9] S.C. Cunha, J.O. Fernandes, Multipesticide residue analysis in maize combining acetonitrile-based extraction with dispersive liquid–liquid microextraction followed by gas chromatography–mass spectrometry, J. Chromatogr. A. 1218 (2011) 7748–7757.

[10] S.R. Rissato, M.S. Galhiane, F.R.N. Knoll, B.M. Apon, Supercritical fluid extraction for pesticide multiresidue analysis in honey: Determination by gas chromatography with electron-capture and mass spectrometry detection, J. Chromatogr. A. 1048 (2004) 153–159.

[11] M.G. Cahill, G. Caprioli, M. Stack, S. Vittori, K.J. James, Semi-automated liquid chromatography-mass spectrometry (LC-MS/MS) method for basic pesticides in wastewater effluents, Anal. Bioanal. Chem. 400 (2011) 587–594.

[12] D.B. Barr, L.L. Needham, Analytical methods for biological monitoring of exposure to pesticides: a review, J. Chromatogr. B. 778 (2002) 5–29.

[13] G. Aragay, F. Pino, A. Merkoçi, Nanomaterials for sensing and destroying pesticides., Chem. Rev. 112 (2012) 5317–38.

[14] C.C. Mayorga-martinez, F. Pino, S. Kurbanoglu, L. Rivas, S.A. Ozkan Iridium oxide nanoparticle induced dual catalytic/inhibition based detection of phenol and pesticide compounds, J. Mater. Chem. B (2014) 2233–2239.

[15] M. Medina-sánchez, C.C. Mayorga-martinez, T. Watanabe, T.A. Ivandini, Y. Honda, F. Pino, K. Nakata, A. Fujishima, Y. Einaga, A. Merkoçi, Corrigendum to 'Microfluidic platform for environmental contaminants sensing and degradation based on boron-doped diamond electrodes' [Biosens. Bioelectron. 08/75 (2015) 365-374].

[16] A. Zamora-Gálvez, A. Ait-Lahcen, L.A. Mercante, E. Morales-Narváez, A. Amine, A. Merkoçi, Molecularly Imprinted Polymer-Decorated Magnetite Nanoparticles for Selective Sulfonamide Detection, Anal. Chem. 88 (2016) 3578–3584.

[17] C.C. Mayorga Martinez, E.F. Treo, R.E. Madrid, C.C. Felice, Biosensors and Bioelectronics Evaluation of chrono-impedance technique as transduction method for a carbon paste / glucose oxidase (CP / GOx) based glucose biosensor, Biosens. Bioelectron. 26 (2010) 1239–1244.

[18] L. Rivas, C.C. Mayorga-martinez, Label-Free Impedimetric Aptasensor for Ochratoxin - A

Detection Using Iridium Oxide Nanoparticles, Anal. Chem. 87 (2015) 5167-5172.

[19] S. Zhu, N. Gan, D. Pan, Y. Li, T. Yang, F. Hu, Y. Cao, D. Wu, Extraction of tributyltin by magnetic molecularly imprinted polymers, Microchim. Acta. 180 (2013) 545–553.

[20] J. He, J. An, D. Zhao, Synthesis and the Characteristics of Iron/Iron Oxide Nanoparticles, IEEE Trans. Magn. 48 (2012) 4293–4296.

[21] K. Petcharoen, A. Sirivat, Synthesis and characterization of magnetite nanoparticles via the chemical co-precipitation method, Mater. Sci. Eng. B. 177 (2012) 421–427.

[22] L. Chen, J. Liu, Q. Zeng, H. Wang, A. Yu, H. Zhang, L. Ding, Preparation of magnetic molecularly imprinted polymer for the separation of tetracycline antibiotics from egg and tissue samples, J. Chromatogr. A. 1216 (2009) 3710–3719.

[23] H. Jung, J.-W. Kim, H. Choi, J.-H. Lee, H.-G. Hur, Synthesis of nanosized biogenic magnetite and comparison of its catalytic activity in ozonation, Appl. Catal. B Environ. 83 (2008) 208–213.

[24] X. Liang, S. Zhu, Y. Zhong, J. Zhu, P. Yuan, H. He, J. Zhang, The remarkable effect of vanadium doping on the adsorption and catalytic activity of magnetite in the decolorization of methylene blue, Appl. Catal. B Environ. 97 (2010) 151–159.

[25] T.Braunbeck, D.E Hinton, B Streit. Fish Ecotoxicology. Basel; Boston: Birkhäuser Verlag,1998

[26] U.S. Epa, Ambient Aquatic Life Water Quality Criteria for Tributyltin (TBT) - Final, (2003).

[27] M.D. Mueller, Tributyltin detection at trace levels in water and sediments using GC with flame-photometric detection and GC-MS, Fresenius' Zeitschrift F{ü}r Anal. Chemie. 317 (1984) 32–36.

[28] J. Wu, Z. Mester, J. Pawliszyn, Determination of tributyltin by automated in-tube solid-phase microextraction coupled with HPLC-ES-MS, J. Anal. At. Spectrom. 16 (2001) 159–165.

[29] M. Xu, X. Luo, J. J. Davis, The label free picomolar detection of insulin in blood serum, Biosens. Bioelectron. 39 (2012) 21–25.

[30] R.-M. Kong, Z.-L. Song, H.-M. Meng, X.-B. Zhang, G.-L. Shen, R.-Q. Yu, A label-free electrochemical biosensor for highly sensitive and selective detection of DNA via a dual-amplified strategy, Biosens. Bioelectron. 54 (2014) 442–447.

[31] M. Medina-Sánchez, B. Ibarlucea, N. Pérez, D. D. Karnaushenko, S. M. Weiz, L. Baraban, G. Cuniberti, O. G. Schmidt, High-performance three-dimensional tubular nanomembrane sensor for DNA detection, Nano Letters 16 (2016) 4288-4296.

[32] A. Benvidi, N. Rajabzadeh, H. Molaye Zahedi, M. MazloumArdakani, M. M. Heidari, L. Hosseinzadeh, Simple and label-free detection of DNA hybridization on a modified graphene nanosheets electrode, Talanta 137 (2015) 80-86.

[33] A. Benvidi, M. D. Tezerjani, S. Jahanbani, M. Mazloum Ardakani, S. M. Moshtaghioun, Comparison of impedimetric detection of DNA hybridization on the various biosensors based on modified glassy carbon electrodes with PANHS and nanomaterials of RGO and MWCNTs, Talanta 147 (2016) 621-627.

FIGURES CAPTIONS

Figure 1. Cartoon of the proposed TBT sensor (A). TEM images of Fe_3O_4NPs (B) and MIP-Fe_3O_4NPs (C). Scale bar: 20 nm.

Figure 2. Comparison of the IR (A) and wide-scan X ray photoelectron (B) spectra of Fe_3O_4NPs (blue) and MIP-Fe_3O_4NPs composite (red). High-resolution X-ray photoelectron spectra of Fe 2p, O 1s, N 1s, C 1s and Si 2p regions of the MIP-Fe_3O_4NPs (C). N_2 adsorption isotherms (left) and dynamic curve (right) of MIP-Fe_3O_4NPs (D). Inset: MIP-Fe_3O_4NPs structure.

Figure 3. Nyquist plot of bare SPE, SPEs modified with MIP-Fe_3O_4NPs and MIP-Fe_3O_4NPs + 5 µM TBT(A). Zeta-potential diagram from the dispersion of MIP-Fe_3O_4NPs and MIP-Fe_3O_4NPs + TBT (B). R_{ct} values obtained for MIP-Fe_3O_4NPs and NIP-Fe_3O_4NPs with and without 5 µM TBT (C). Calibration curve for R_{ct} values as a function of the TBT concentration (D). Nyquist plot of TBT, MBT and DBT at the same concentration (5µM)(E).

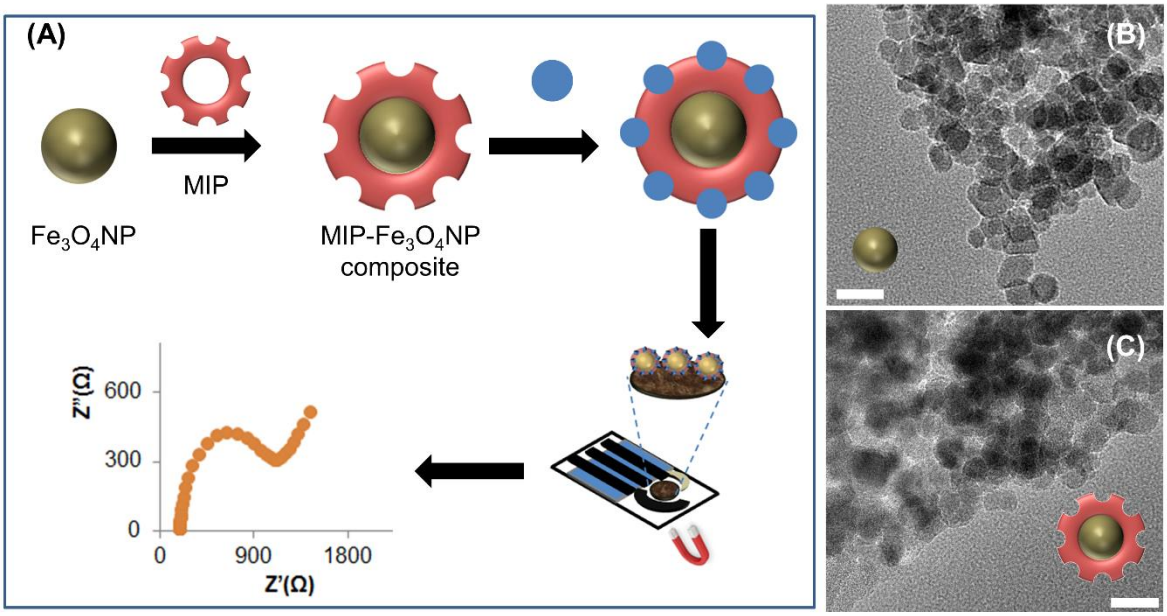
(A)
MIP
Fe3O4NP
MIP-Fe3O4NP
composite
Z''(Ω)
600
300
0
0
900
1800
Z'(Ω)
(B)
(C)

Figure 1

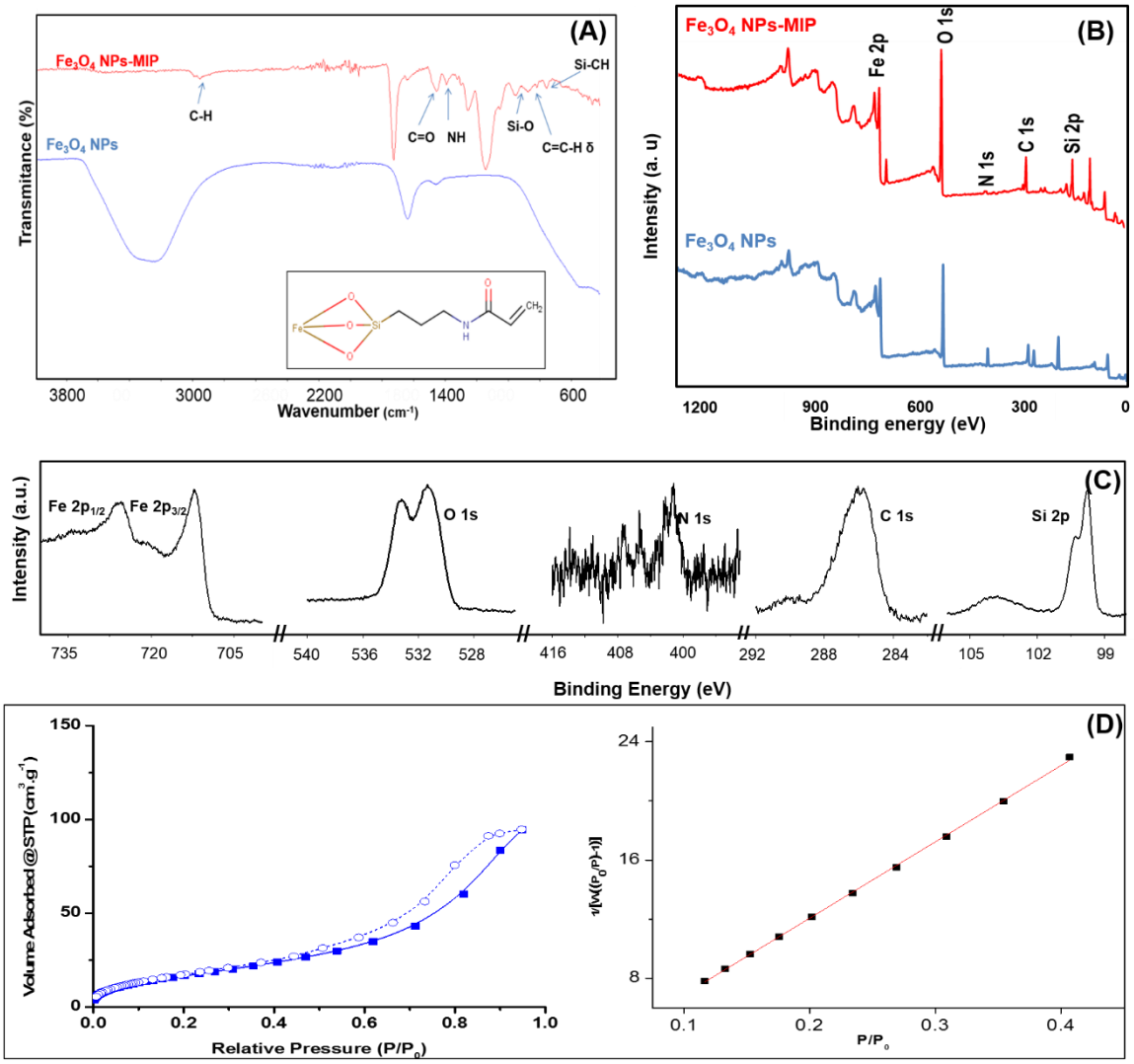
(A)
Fe3O4 NPs-MIP
Fe3O4 NPs
C-H
C=O
NH
Si-O
Si-CH
C=C-H δ
Transmitance (%)
Wavenumber (cm-1)
(B)
Fe3O4 NPs-MIP
Fe3O4 NPs
Fe 2p
O 1s
N 1s
C 1s
Si 2p
Intensity (a. u)
Binding energy (eV)
(C)
Fe 2p1/2
Fe 2p3/2
O 1s
N 1s
C 1s
Si 2p
Intensity (a.u.)
Binding Energy (eV)
(D)
Volume Adsorbed @STP (cm3.g-1)
Relative Pressure (P/P0)
1/[W((P0/P)-1)]
P/P0

Figure 2

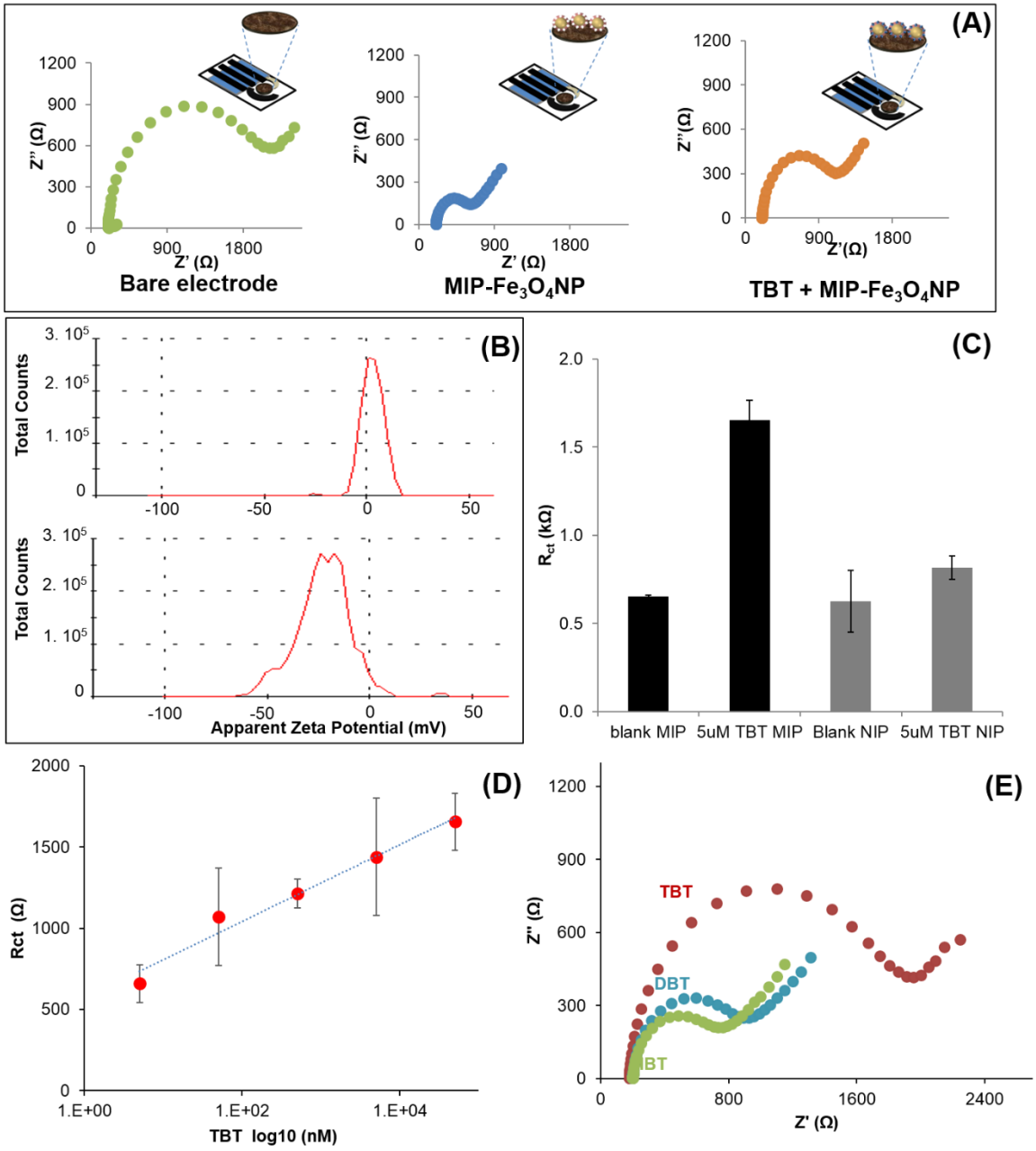
(A)
Z'' (Ω)
Z' (Ω)
Bare electrode
MIP-Fe3O4NP
TBT + MIP-Fe3O4NP
(B)
Total Counts
Apparent Zeta Potential (mV)
(C)
Rct (kΩ)
blank MIP
5uM TBT MIP
Blank NIP
5uM TBT NIP
(D)
Rct (Ω)
TBT log10 (nM)
(E)
TBT
DBT
BT

Figure 3